Turkish Journal of Engineering

Turkish Journal of Engineering (TUJE)
Vol. 4, Issue 4, pp. 209-217, October 2020
ISSN 2587-1366, Turkey
DOI: 10.31127/tuje.648882
Research Article

EFFECTIVE ADSORPTION OF TETRACYCLINE WITH Co_3O_4/Fe_3O_4 BIMETALLIC NANOPARTICLES

Muhammed Musa [1], Hatice Hasan [1], Hülya Malkoç [1], Memduha Ergüt *[1], Deniz Uzunoğlu [1] and Ayla Özer [1]

[1] Mersin University, Engineering Faculty, Department of Chemical Engineering, Mersin, Turkey
ORCID ID 0000 – 0002 – 8646 – 8354
mihemedmousa@gmail.com

[1] Mersin University, Engineering Faculty, Department of Chemical Engineering, Mersin, Turkey
ORCID ID 0000 – 0002 – 4643 – 1282
haticehasan97@hotmail.com

[1] Mersin University, Engineering Faculty, Department of Chemical Engineering, Mersin, Turkey
ORCID ID 0000 – 0003 – 0572 – 6727
hulyajt@gmail.com

[1] Mersin University, Engineering Faculty, Department of Chemical Engineering, Mersin, Turkey
ORCID ID 0000 – 0001 – 7297 – 1533
memduha.ergut@gmail.com

[1] Mersin University, Engineering Faculty, Department of Chemical Engineering, Mersin, Turkey
ORCID ID 0000 – 0001 – 9706 – 303X
duzunoglu@mersin.edu.tr

[1] Mersin University, Engineering Faculty, Department of Chemical Engineering, Mersin, Turkey
ORCID ID 0000 – 0002 – 7824 – 238X
ayozer@mersin.edu.tr

* Corresponding Author
Received: 20/11/2019 Accepted: 31/01/2020

ABSTRACT
In the present study cobalt oxide/iron oxide bimetallic nanoparticles (Co_3O_4/Fe_3O_4 NPs) were synthesized by chemical co-precipitation method. The synthesized Co_3O_4/Fe_3O_4 NPs were characterized by SEM and XRD analysis. The synthesized nanoparticles were used as an adsorbent for the removal of a kind of antibiotic as Tetracycline (TC) from aqueous solutions. According to characterization results, small plate-like structures and agglomerated irregular spherical nanosized particles (101.85 ± 15.04 nm) were formed. The XRD data confirmed the structure of synthesized adsorbent was Co_3O_4/Fe_3O_4. The optimum tetracycline adsorption conditions were determined as the initial pH of solution 9.0, temperature 55°C, and adsorbent concentration 3.0 g/L. A linear increase was observed in equilibrium uptakes of TC with the increasing the initial antibiotic concentrations. The experimental equilibrium data was modelled with Langmuir and Freundlich isotherm models. The experimental equilibrium data was the best agreement to the Langmuir isotherm model. The maximum monolayer coverage capacity of Co_3O_4/Fe_3O_4 NPs for TC adsorption was found to be 149.26 mg/g at 55°C optimum temperature. The experimental kinetic adsorption data were defined as the best agreement with the pseudo-second-order kinetic model. Weber Morris mass transfer modelling results showed that both the film (boundary layer) and intra-particle diffusion were effective in the adsorption process. The thermodynamic studies suggested that the adsorption process was endothermic, spontaneous and the positive ΔS value indicated increased disorder at the solid-solution interface during the adsorption. Moreover, the synthesized adsorbent showed high adsorption efficiencies at the end of seven sequence usages.

Keywords: *Adsorption, Bimetallic Nanoparticles, Cobalt Oxide, Iron Oxide, Tetracycline Removal*

1. INTRODUCTION

Antibiotics a kind of significant pharmaceutical ingredient, have been used for many decades as both human and veterinary medicines (Cao *et al.*, 2018).

Tetracycline (TC, $C_{22}H_{24}N_2O_8$) is the second most widely used antibiotics family in the world. TCs are often used in human therapy and livestock industry due to their broad-spectrum antimicrobial activity against a variety of pathogens (Erşan *et al.*, 2013; Bao *et al.*, 2013).

However, nowadays, the presence of antibiotics in the environment and their potential threat to human health and aquatic ecology has led to great concerns. Because antibiotics taken by humans and animals are not completely absorbed in the body. It has been suggested that about 90% of an administrated dose of antibiotic may be excreted through urine and feces (Turku *et al.*, 2007). In addition, the removal of these drug residues reaching sewage treatment plants cannot be fully achieved due to their resistance to biological degradation. Therefore, antibiotic residues can easily mix with surface and ground waters. They also pose a risk for ecological and aquatic environments due to their toxic effects and long half-life (Zhao *et al.*, 2011; Güler, 2016).

It has been reported that the antibiotics concentrations in untreated domestic wastewater range between 100 ng/L and 6 µg/L, while the concentrations in pharmaceutical and hospital wastewater can reach up to 100–500 mg/L (Cao *et al.*, 2018).

Therefore, the treatment of wastewater containing antibiotic residues with high organic load is one of the important environmental problems. So, it is necessary to develop inexpensive and efficient treatment methods for this purpose.

The oxidation methods, membrane filtration, reverse osmosis, ultrafiltration, Fenton process, and adsorption are applied as alternative treatment methods for the removal of antibiotics from wastewaters. Adsorption is commonly believed the easiest and cheapest one among these techniques.

Graphene oxide (Gao *et al.*, 2012), carbon nanotubes (Ji *et al.*, 2010), silica (Turku *et al.*, 2007), kaolinite (Li *et al.*, 2010), goethite (Zhao *et al.*, 2011), clay mineral illite (Chang *et al.*, 2012), montmorillonite (Parolo *et al.*, 2008); biosorbents such as maize stalks (Balarak *et al.*, 2016), *Pachydictyon coriaceum* and *Sargassumhemiphyllum* (Li *et al.*, 2015); activated carbon (Martins *et al.*, 2015), chitosan (Kang *et al.*, 2010); composite materials such as Fe_3O_4@SiO_2-Chitosan/graphene oxide nanocomposite (Huang *et al.*, 2017), Heteropolyacid–chitosan/TiO_2 composites (Yu *et al.*, 2014); nanomaterials such as Co-doped UiO-66 nanoparticle (Cao *et al.*, 2018) and Fe/Ni bimetallic nanoparticles (Dong *et al.*, 2018), and cobalt ferrite nanoparticles (Zhao *et al.*, 2014) were used as adsorbents for the removal of TC.

The aim of this work synthesis and characterization of bimetallic Co_3O_4/Fe_3O_4 NPs and investigate the adsorption of TC on Co_3O_4/Fe_3O_4 NPs. In this study, the experimental parameters that affect the adsorption of TC on Co_3O_4/Fe_3O_4 NPs such as initial pH of the solution, adsorbent concentration, initial TC concentration, and temperature were optimized to obtain maximum TC removal yield and also, the reusability of adsorbent was tested. The thermodynamic, equilibrium, kinetic, and mass transfer modeling studies were also carried out to evaluate the adsorption process.

2. MATERIALS AND METHODS

2.1. Materials

All of the chemicals were of analytical grade and they were used without further purification. For the synthesis of Co_3O_4/Fe_3O_4 bimetallic nanoparticles, $Fe(NO_3)_2.9H_2O$ and $Co(NO_3)_2.6H_2O$ were supplied from Across. Tetracycline hydrochloride ($C_{22}H_{24}N_2O_8.HCl$) was purchased from Sigma Aldrich. The chemical structure of TC antibiotics was presented in Fig. 1.

A stock solution of 250 mg/L of Tetracycline (TC) was first prepared and then the desired antibiotic concentrations were prepared by appropriate dilutions from the stock solution. The initial pHs of the solutions was adjusted with 0.1 N hydrochloric acid and/or 0.1 N sodium hydroxide.

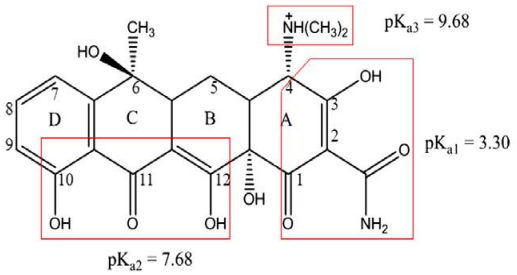

Fig.1. The structure of tetracycline, the framed regions represents the structural moieties associated with the three acidic dissociation constants (pKa).

2.2. Synthesis and Characterization of Co_3O_4/Fe_3O_4 NPs

The synthesis of Co_3O_4/Fe_3O_4 bimetallic nanoparticles (Co_3O_4/Fe_3O_4 NPs) was carried out by the chemical co-precipitation method. In the experiments, 25 mL of 0.1 M $Fe(NO_3)_2.9H_2O$ and 25 mL of 0.2 M $Co(NO_3)_2.6H_2O$ solution were mixed at room temperature for 15 min. Then 1.0 M sodium hydroxide solution was slowly added to the prepared solution. This mixture constantly stirred until the pH of 11.0 was reached. The changing of the color of the salt solution to intense black indicated the formation of Co_3O_4/Fe_3O_4 NPs. The obtained final mixture was kept under vigorous stirring for 3 h at 90°C. The formed nanoparticles were separated by centrifugation and then collected nanoparticles were washed several times with deionized water and dried in an oven at 105°C overnight.

The morphology of the Co_3O_4/Fe_3O_4 NPs was analyzed by Scanning Electron Microscope (SEM) analysis with Zeiss/Supra 55 SEM and the crystal structure was determined by X-ray Powder Diffraction (XRD) analysis, using nickel-filtered Cu Kα radiation in a Philips XPert MPD apparatus operated at 40 kV and 30 mA, in the 2θ range of 10°–90°.

2.3. Adsorption Studies

The batch adsorption experiments were carried out in 250 mL Erlenmeyer flasks containing 100 mL of TC

antibiotic solution. 0.1 g of adsorbent, except for adsorbent concentration experiments, was contacted with 100 mL of TC solution at known initial antibiotic concentration and initial pH of solutions. Then the flasks were agitated at a constant temperature and shaking rate. Samples were taken before mixing the Co_3O_4/Fe_3O_4 NPs and TC solution and at pre-determined time intervals for the unadsorbed antibiotic concentration in the solution. Samples were centrifuged and the supernatant liquid was analyzed by UV-vis spectrophotometer at the wavelength of 360 nm.

The adsorbed amount of TC [q_e; (mg/g)] and the percentage of adsorption [Adsorption (%)] at equilibrium were calculated with Eqs. (1) and (2) as presented follows:

$$q_e\ (mg/g) = \frac{C_0 - C_e}{m} \cdot V \quad (1)$$

$$\text{Adsorption } (\%) = [\frac{(C_0 - C_e)}{C_0}] \cdot 100 \quad (2)$$

Where C_o (mg/L) and C_e (mg/L) are the initial and equilibrium concentrations of TC solution, respectively; and m(g) is the mass of adsorbent, and V(L) is the volume of the liquid phase.

3. RESULTS AND DISCUSSIONS

3.1. The Characterization of Co_3O_4/Fe_3O_4 NPs

The morphology of Co_3O_4/Fe_3O_4 NPs before and after adsorption was determined by SEM analysis and SEM images obtained at different magnifications were presented in Fig. 2. (a – d). SEM images of the synthesized Co_3O_4/Fe_3O_4 NPs (Fig. 2 (a, b)) showed that highly clustered surfaces, and agglomerated irregular spherical particles were formed. The SEM images obtained after the adsorption process showed that the morphology of Co_3O_4/Fe_3O_4 NPs changed a bit slightly; the clustered surfaces were disappeared, and the nanosized, spherical, and agglomerated particles became more apparent.

The mean particle size of the synthesized Co_3O_4/Fe_3O_4 NPs was calculated by using the modified form of the Williamson–Hall method, as presented following Eq. (3):

$$\beta\cos(\theta) = k\lambda/D + 4\text{Ɛ}\sin(\theta) \quad (3)$$

Where 'λ' is the wavelength of X-Ray (0.1541 nm), 'β' is FWHM (full width at half maximum), 'θ' is the diffraction angle, Ɛ is the strain, k is shape factor (0.9) and 'D' is mean particle diameter size.

The strain and particle size are calculated from the slope and y-intercept (kλ/D) of Williamson–Hall plot, i.e. the plot of between 4sin(θ) and βcos(θ). The slope of the graph gives strain and the intercept on the βcos(θ) axis gives the mean particle size corresponding to zero strain (Mote *et al.*, 2012). The mean particle size of Co_3O_4/Fe_3O_4 NPs was calculated to be 57.75 nm by using the Williamson–Hall method.

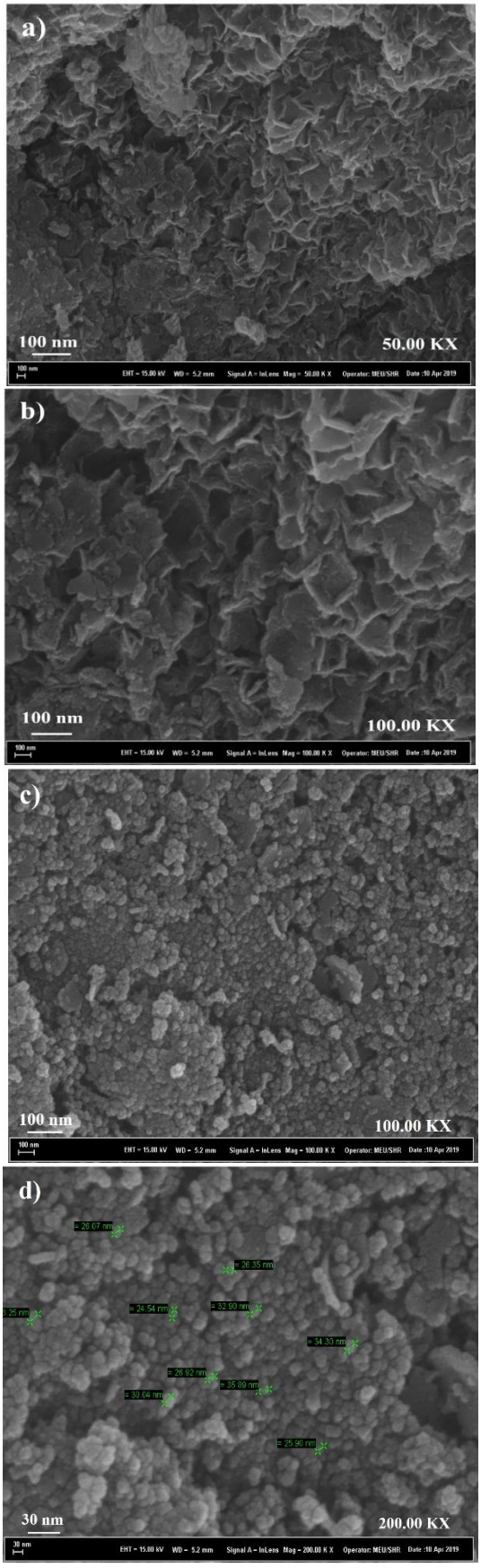

Fig.2. SEM images obtained at different magnifications before a) 50 KX, b)1000 KX; after c) 100 KX, d) 200 KX.

The mean particle size of the spherical particles was determined as 101.85 ± 15.04 nm by using the Image J program utilizing randomly selected particles from SEM images after the adsorption process.

The larger mean particle size of the Co_3O_4/Fe_3O_4 NPs was obtained from the SEM images than that obtained from XRD data. The reason for this result may be due to the fact that the SEM images indicate the size of polycrystalline particles which show the tendency to agglomerate due to their high surface energy.

The XRD pattern of synthesized Co_3O_4/Fe_3O_4 NPs was presented in Fig. 3.

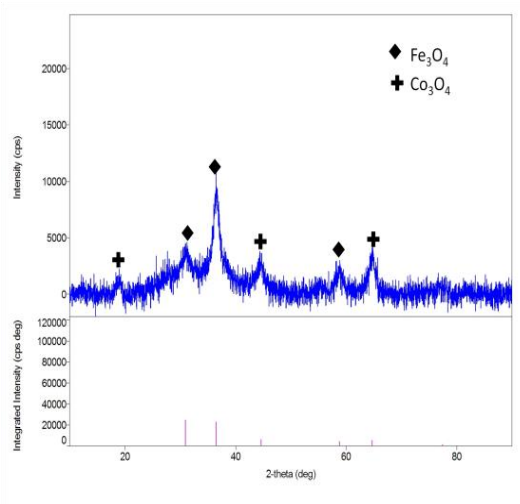

Fig.3. XRD diagram of synthesized Co_3O_4/Fe_3O_4 NPs

The peaks at 2θ = 30.91°, 36.46°, and 58.83° correspond to Fe_3O_4 and the peaks at 2θ = 19.02°, and 44.59°, and 64.46° showed the Co_3O_4 phase (Manigandan *et al.*, 2013).

3.2. Effects of Environmental Conditions on the Adsorption

3.2.1. Effect of initial pH

The initial pH is one of the most important parameters affecting the adsorption of TC on the active adsorbent surface. The interaction between the TC molecules and the adsorbent is mainly dependent on the TC species and variation of the surface loading of the adsorbent.

The isoelectric point (pH_{IEP}) of Co_3O_4/Fe_3O_4 NPs was determined by solid addition method at different pH (3.0 - 12) values (Uzunoğlu *et al.*, 2016). The variation of the isoelectric point with pH was presented in Fig. 4.

TC molecules are very sensitive to the initial pH of the solution due to their protonation status. As shown in Fig. 4, the isoelectric point at which the surface electrical charge of Co_3O_4/Fe_3O_4 NPs changes from negative to positive value was found to be pH 8.47.

Accordingly, the surface of Co_3O_4/Fe_3O_4 NPs was charged negatively below pH 8.47 and positively charged above this pH value. However; the structure of TC contains many polar and ionizable groups, including amino, carboxyl, phenol, alcohol, and ketone. The TC molecules can be present in three forms, cationic (pH<3.3), zwitterionic (3.3<pH<7.7) and anionic (pH>7.7) in aqueous solutions at different pH values (Roca Jalil *et al.*, 2018). In this case, there is an electrostatic interaction depending on the initial pH values in the adsorption of TC on Co_3O_4/Fe_3O_4 NPs surface. The effect of initial pH on the adsorption of TC to Co_3O_4/Fe_3O_4 NPs was given in Fig. 5.

As shown in Figure 5, the highest adsorption capacity was obtained at the initial pH: 9.0. At pH: 9.0, the TC molecules are in anionic form, while the adsorbent surface is positively charged. Therefore, the amount of TC adsorbed is the highest due to the increased electrostatic attraction between the TC molecules and the adsorbent surface at pH: 9.0.

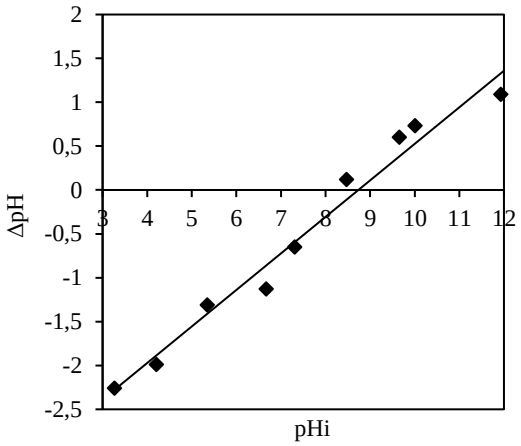

Fig.4. The isoelectric point of Co_3O_4/Fe_3O_4 NPs

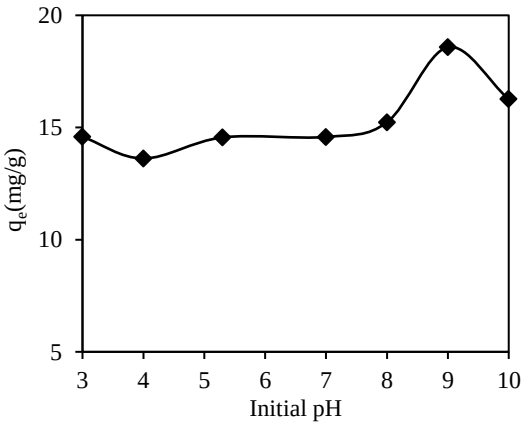

Fig.5. Effect of initial pH on the adsorption of TC (Co=50 mg/L; Xo=1.0 g/L; T=25 °C; t= 420 min)

3.2.2. Effect of initial TC concentration

The effect of initial antibiotic concentration on adsorption was depicted in Fig. 6. As can be seen from Fig. 6, the adsorption capacities increased linearly (q_e=0.3047*C_o, R^2=0.999) in the studied TC concentrations as a result of the increase in the driving force (ΔC) to get over mass transfer resistances of the pollutant between the aqueous and solid phases.

3.2.3. Effect of adsorbent concentration

The adsorbent concentration effect on the equilibrium uptake was presented in Fig.7. According to Fig. 7, a

decrease was observed in adsorption capacity by increasing the adsorbent concentration from 0.5 g/L to 3.0 g/L. However, the adsorption percentages increased by increasing the adsorbent concentration values. Therefore, although the highest adsorption capacity for tetracycline antibiotic was obtained at 0.5 g/L of adsorbent concentration, the optimum adsorbent concentration was determined as 3.0 g/L, since the highest removal yield was obtained at this adsorbent concentration value.

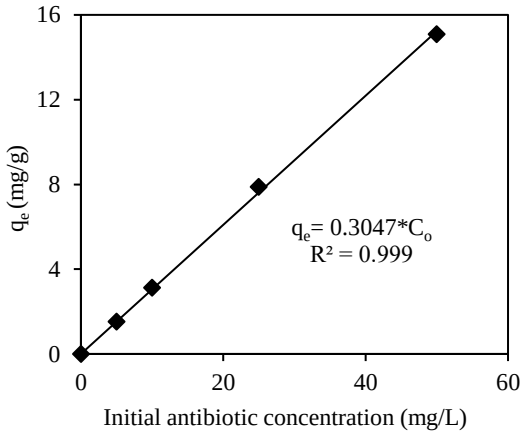

Fig.6. Effect of initial antibiotic concentration on the adsorption of TC (pH=9.0; Xo=3.0 g/L; T=50 °C; t=420 min)

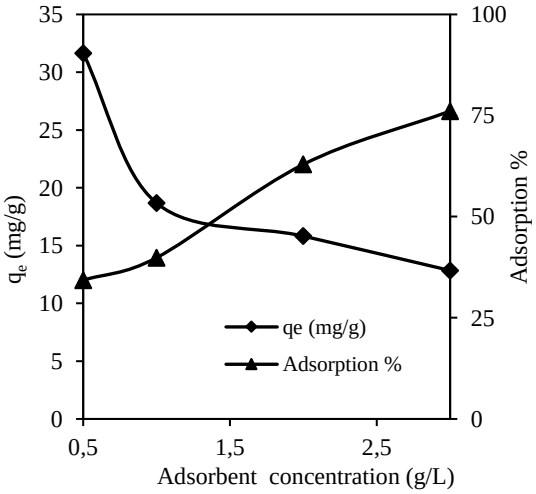

Fig.7. Effect of adsorbent concentration on the adsorption of TC (Co=50 mg/L, pH=9.0; T=25 °C; t=420 min)

3.2.4. Effect of temperature

The effect of temperature was presented in Fig. 8. According to Fig. 8, the increase in temperature has a positive effect on the adsorption of TC. The obtained adsorption capacities were increased with the increase in temperature from 25°C to 65°C. This result indicated that the studied adsorption process was endothermic nature.

Also, it was observed that when the temperature was increased from 55°C to 65°C, a slight change was obtained on adsorption capacity. So, the adsorption capacities approximately became constantly after 55°C. Therefore, the optimum temperature value for TC adsorption was determined to be 55°C.

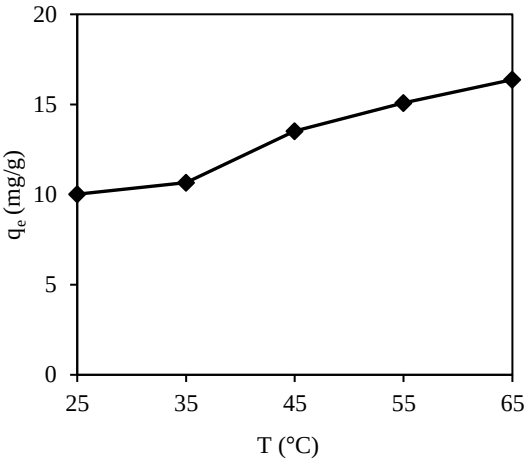

Fig. 8. Effect of temperature on the adsorption of TC (Co= 50 mg/L, pH=9.0; Xo=3.0 g/L; t=420 min)

3.3. Thermodynamic Parameters

The temperature effect was also confirmed with thermodynamic studies by calculating the entropy change (ΔS), enthalpy change (ΔH), and Gibbs energy change (ΔG). ΔH and ΔS were calculated from the slope and intercept of the linear plot of ln K_c versus 1/T according to Van't Hoff equation (Eq. 4), while ΔG was calculated according to Eq. 5.

$$\ln K_c = \left(\frac{\Delta S}{R}\right) - \left(\frac{\Delta H}{R}\right) \cdot \frac{1}{T} \quad (4)$$

$$\Delta G = -RT \ln Kc = \Delta H - T\Delta S \quad (5)$$

In this study, the linear form of Van't Hoff equation for the adsorption of TC onto Co_3O_4/Fe_3O_4 NPs was found as $\ln K_c = -8502.2 \times \frac{1}{T} + 28.569$ with the regression coefficient 0.993 (data not shown) and the thermodynamic parameters were calculated and presented in Table 1. According to Table 1, the calculated ΔG values had negative indicating that adsorption was spontaneous. The positive value of ΔS suggested that randomness of the adsorbed TC species at the solid-solution interface during adsorption and the studied adsorption systems were endothermic (ΔH>0).

Table 1. Thermodynamic parameters of adsorption

Thermodynamic parameters				
T (K)	*Kc*	*ΔH (kJ/mol)*	*ΔS (kJ/mol.K)*	*ΔG (kJ/mol)*
298	1.1132	70.68	0. 237	-0.265
318	5.6439			-4.575
328	12.824			-6.957
338	34.555			-9.955

3.4. The reusability of adsorbent

The operation cost is one of the important issues that need to be carefully considered. Therefore, operation cost can be significantly reduced owing to adsorbent reusability in practical applications. The reusability of the adsorbent was evaluated through seven recycled tests. The results regarding the TC adsorption efficiency for seven cycles of the adsorbent were given in Fig. 9. Between each cycle of use, the adsorbent was separated from the solution with Whatman #1 filter paper, washed several times with deionized water and then applied for the next experiment without any modifications. After each recycling test, the adsorption percentage of TC was determined. As seen in Fig. 9, the adsorption % of TC declined slightly from 99.43% in the first cycle to 88.42% after seven cycles of adsorption for 10 mg/L of TC solution. This result showed that the adsorbent can be recycled and reused for at least seven successive cycles without any significant loss of its efficiency.

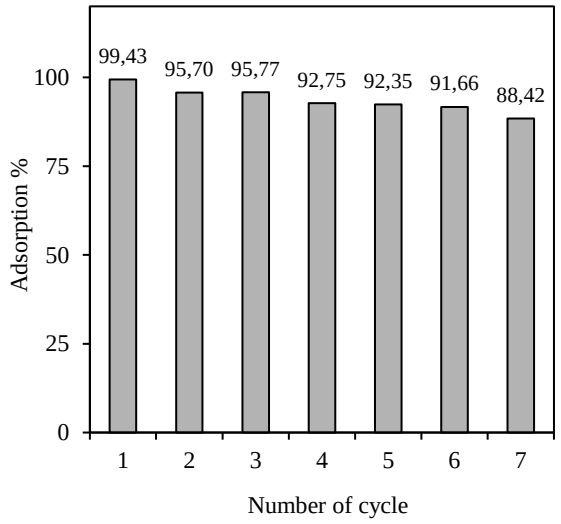

Fig. 9. Reusability of adsorbent within experimental runs for seven successive cycles (Co=10 mg/L, pH=9.0; Xo=3.0 g/L; t=420 min)

3.5. Equilibrium, Kinetic, and Mass Transfer Modelling

3.5.1. Equilibrium modeling

The well-known linearized forms of the Langmuir and Freundlich isotherm models were used to describe the adsorption equilibrium. The linearized forms of Langmuir and Freundlich isotherm models were given in Eqs. (6) and (7):

Langmuir: $$\frac{1}{q_e} = \frac{1}{Q^\circ b} \cdot \frac{1}{C_e} + \frac{1}{Q^\circ} \quad (6)$$

Freundlich: $$\ln q_e = \ln K_F + \left(\frac{1}{n}\right) \ln C_e \quad (7)$$

Langmuir isotherm model based on the assumption of maximum adsorption corresponds to a saturated monolayer of adsorbed molecules on the adsorbent surface with constant energy. Freundlich isotherm model suggests non-ideal sorption that involves heterogeneous surface energy systems (Malik, 2004).

The isotherm constants with regression coefficients (R^2) were presented in Table 2. Also, the experimental and predicted isotherms for adsorption at 55°C was given in Fig. 10.

According to Table 2 and Fig. 10, the Langmuir isotherm model was better fitted to experimental equilibrium data. This result showed that the adsorption occurred at specific homogeneous sites within the adsorbent forming monolayer coverage of TC at the surface of Co_3O_4/Fe_3O_4 NPs. The maximum monolayer coverage capacity of Co_3O_4/Fe_3O_4 NPs was determined as 149.26 mg/g at 55°C which is the optimum temperature. Moreover, as seen in Table 2, the maximum monolayer coverage capacity values of the adsorbent for TC increased by increasing temperature may be due to the endothermic nature of the studied adsorption process. The comparison of Q^o values of various types of adsorbents for TC adsorption was presented in Table 3.

Accordingly, it was seen that the adsorption capacity of Co_3O_4/Fe_3O_4 NPs was comparable with other adsorbents reported in earlier studies.

Table 2. The constants of the adsorption isotherm models with regression coefficients (pH=9.0; Xo=3.0 g/L; t=420 min)

T (°C)	Langmuir isotherm model			Freundlich isotherm model		
	Q^o (mg/g)	b (L/mg)	R^2	K_F (mg/g)/(L/mg)1/n)	1/n	R^2
25	21.053	0.03536	0.999	1.0114	0.6988	0.995
35	55.249	0.01745	0.998	1.0443	0.8627	0.991
45	135.135	0.01380	0.997	1.9397	0.8699	0.979
55	149.254	0.01020	0.999	1.4745	1.0089	0.994

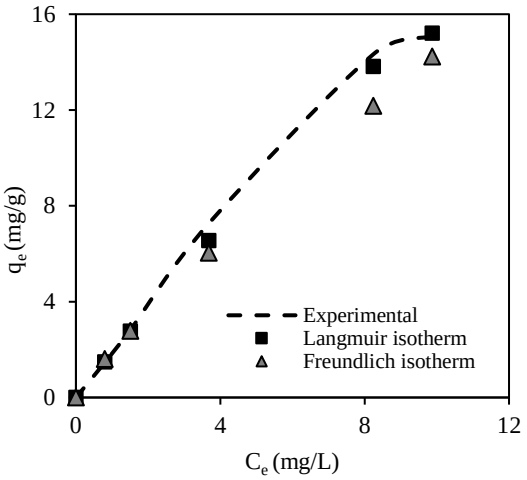

Fig.10. The comparison of the experimental and predicted isotherms

Table 3. The maximum monolayer adsorption capacity values (Q°) of various types of adsorbents in the literature

Adsorbent	Q° (mg/g)	Reference
Fe_3O_4@SiO_2-Chitosan/GO	151.4	(Huang *et al.*, 2017)
NH_2-MIL 101(Cr)	14	(Tian *et al.*, 2016)
Zn-AC	51.65	(Takdaştan *et al.*, 2016)
Cu_2O-TiO_2-Pal	113.6	(Shi *et al.*, 2016)
$GBCM_{350}$ activated carbon	58.2	(Álvarez-Torrellas *et al.*, 2016)
Co_3O_4/Fe_3O_4 NPs	149.25	This study

3.5.2. Kinetic modeling

The adsorption kinetics was elucidated by correlating the adsorption kinetic data using the linear forms of the Lagergen's pseudo-first-order and the pseudo-second-order kinetic models. The linearized forms of pseudo-first-order and the pseudo-second-order kinetic models were given in Eqs. (8) and (9), respectively (Mall *et al.*, 2007):

$$\text{Pseudo first order: } \log(q_e - q_t) = \log(q_e) - \frac{k_1 t}{2.303} \quad (8)$$

$$\text{Pseudo second order : } \frac{t}{q_t} = \left(\frac{1}{q_e^2 k_2}\right) + \frac{t}{q_e} \quad (9)$$

For the adsorption of TC onto Co_3O_4/Fe_3O_4 NPs, the parameters of the pseudo-first-order and pseudo-second-order kinetic models with regression coefficients were presented in Table 4. From Table 4, higher values of R^2 and the consistency between experimental and calculated uptake values showed a better agreement of the pseudo-second-order kinetics.

3.5.3. Effect of mass transfer

Weber-Morris model was used to determine the boundary layer and intra-particle diffusion mechanism between TC and adsorbent. Weber-Morris intraparticle diffusion model is expressed by the following Eq.(10) ;

$$q_t = K_i . t^{0.5} + I \quad (10)$$

In Weber-Morris equation; I is the intercept related to the boundary layer effect and K_i is the intraparticle diffusion rate constant which can be evaluated from the slope of the linear plots of qt versus $t^{0.5}$. According to this model, if the only intraparticle diffusion is the rate-controlling step in the adsorption process, the plot of uptake (q_e) versus the $t^{0.5}$ should be linear and these lines pass through the origin. On the other side, the Weber-Morris plot can be linear and also has an intercept value if the adsorption system follows both intraparticle and film diffusion (Wu *et al.*, 2009). The model parameters and regression coefficients were summarized in Table 4. Based on the results, it was observed a multilinear plot (figure not shown) indicated that both intraparticle and film diffusion were effective on the adsorption. Moreover, according to Table 4; it was seen that the internal (Ki) and external diffusion constants (I) gradually increased with increasing initial contaminant concentration.

Table 4. Kinetic and intra-particle mass transfer model parameters (pH=9.0, Xo=3g/L, t=420 min)

Co (mg/L)	qe, exp (mg/g)	Pseudo-first-order			Pseudo-second-order			Weber-Morris Model		
		k_1 (min^{-1})	qe,cal_1 (mg/g)	R^2	k_2 (g/mg.min)	qe,cal_2 (mg/g)	R^2	Ki ($mg/g.min^{0.5}$)	I	R^2
5	2.503	0.003685	2.3637	0.936	0.002233	2.749	0.970	0.0332	0.8925	0.995
10	3.163	0.004376	2.2014	0.960	0.004520	3.300	0.995	0.1009	0.9907	0.982
25	7.879	0.008521	7.3198	0.954	0.002852	8.453	0.991	0.3489	1.1454	0.990
50	15.086	0.005758	13.3967	0.919	0.00071	17.065	0.972	0.563	1.9738	0.998

4. CONCLUSION

In this study, Co_3O_4/Fe_3O_4 NPs were synthesized by the co-precipitation method for the removal of TC which is a kind of antibiotic from the aqueous solutions. The characterization studies of Co_3O_4/Fe_3O_4 NPs were carried out by SEM and XRD analysis. According to XRD results, the peaks were obtained correspond to Fe_3O_4 and Co_3O_4.

The adsorption was highly dependent on initial pH, adsorbent concentration, initial TC concentration, and temperature. The kinetics of TC adsorption on Co_3O_4/Fe_3O_4 NPs follows the pseudo-second-order model. The equilibrium data fitted well in the Langmuir model of adsorption, showing monolayer coverage of TC molecules at the outer surface of Co_3O_4/Fe_3O_4 NPs. The maximum monolayer coverage capacity of Co_3O_4/Fe_3O_4 NPs for TC adsorption determined to be 149.26 mg/g. Both intraparticle and film diffusion effects were determined on the adsorption process. Moreover, the adsorbent showed reusability at least seven sequence usages without loss of adsorbent property. The TC adsorption onto Co_3O_4/Fe_3O_4 NPs was found to be feasible and spontaneous from thermodynamic studies.

Consequently, these results provided the synthesis of an efficient adsorbent for the effective removal of antibiotic contaminants like tetracyclene in wastewater.

NOMENCLATURE

b : A constant related to the affinity of the binding sites (L/mg)
C_e : Unadsorbed Cr(VI) metal ion concentration at equilibrium (mg/L)
C_o : Initial Cr(VI) metal ion concentration (mg/L)
K_F : Freundlich constant indicating adsorption capacity ((mg/g)/(L/mg)$^{1/n}$)
K_i : Intraparticle diffusion rate constant (mg/g.min$^{0.5}$)
k_1 : Pseudo first order kinetic rate constant (1/min)
k_2 :Pseudo second order kinetic rate constant (g/mg.min)
q_e :Adsorbed amount per unit mass of adsorbent (mg/g)
q_{e,cal_1} :Calculated adsorbed amount per unit mass of adsorbent from pseudo first order kinetic model (mg/g)
q_{e,cal_2} :Calculated adsorbed amount per unit mass of adsorbent from pseudo second order kinetic model (mg/g)
$q_{e,exp}$:Experimental adsorbed amount per unit mass of adsorbent (mg/g)
q_t :Adsorbed amount per unit mass of adsorbent at any time (mg/g)
Q_o :Maximum monolayer coverage capacity of adsorbent (mg/g)
1/n : Freundlich constant indicating adsorption intensity

REFERENCES

Álvarez-Torrellas, S., Ribeiro, R. S., Gomes, H. T., Ovejero, G., & García, J. (2016). "Removal of antibiotic compounds by adsorption using glycerol-based carbon materials". *Chemical Engineering Journal*, Vol. 296, pp. 277-288.

Balarak, D., Mostafapour, F. K., & Azarpira, H. (2016). "Adsorption isotherm studies of tetracycline antibiotics from aqueous solutions by maize stalks as a cheap biosorbent." *International Journal of Pharmacy and Technology*, Vol. 8, No. 3, pp. 16664-16675.

Bao, X., Qiang, Z., Ling, W., & Chang, J. H. (2013). "Sonohydrothermal synthesis of MFe_2O_4 magnetic nanoparticles for adsorptive removal of tetracyclines from water." *Separation and Purification Technology*, Vol.117, pp.104-110.

Cao, J., Yang, Z. H., Xiong, W. P., Zhou, Y. Y., Peng, Y. R., Li, X., ... & Zhang, Y. R. (2018). "One-step synthesis of Co-doped UiO-66 nanoparticle with enhanced removal efficiency of tetracycline: Simultaneous adsorption and photocatalysis." *Chemical Engineering Journal*, Vol. 353, pp.126-137.

Chang, P. H., Li, Z., Jean, J. S., Jiang, W. T., Wang, C. J., & Lin, K. H. (2012). "Adsorption of tetracycline on 2: 1 layered non-swelling clay mineral illite." *Applied Clay Science*, Vol. 67, pp. 158-163.

Dong, H., Jiang, Z., Zhang, C., Deng, J., Hou, K., Cheng, Y., ... & Zeng, G. (2018). "Removal of tetracycline by Fe/Ni bimetallic nanoparticles in aqueous solution." *Journal of colloid and interface science*, Vol. 513, pp. 117-125.

Erşan, M., Bağda, E., & Bağda, E. (2013). "Investigation of kinetic and thermodynamic characteristics of removal of tetracycline with sponge like, tannin based cryogels." *Colloids and surfaces B: Biointerfaces*, Vol. 104, pp. 75-82.

Gao, Y., Li, Y., Zhang, L., Huang, H., Hu, J., Shah, S. M., & Su, X. (2012). "Adsorption and removal of tetracycline antibiotics from aqueous solution by graphene oxide." *Journal of colloid and interface science*, Vol. 368, No.1, pp.540-546.

Güler, Ü. A. (2016). "Aljinat-TiO_2-Alg Kompozitinin Sentezi ve Sulu Çözeltilerden Tetrasiklin Gideriminde Kullanılabilirliği ve Karakterizasyonu." *Karaelmas Science and Engineering Journal*, Vol. 6, No.1, pp. 130-135.

Huang, B., Liu, Y., Li, B., Liu, S., Zeng, G., Zeng, Z., ... & Yang, C. (2017). "Effect of Cu (II) ions on the enhancement of tetracycline adsorption by Fe_3O_4@SiO_2-Chitosan/graphen oxide nanocomposite." *Carbohydrate polymers*, Vol. 157, pp. 576-585.

Ji, L., Chen, W., Bi, J., Zheng, S., Xu, Z., Zhu, D., & Alvarez, P. J. (2010). "Adsorption of tetracycline on single-walled and multi-walled carbon nanotubes as affected by aqueous solution chemistry." *Environmental toxicology and chemistry*, Vol. 29, No. 12, pp. 2713-2719.

Kang, J., Liu, H., Zheng, Y. M., Qu, J., & Chen, J. P. (2010). "Systematic study of synergistic and antagonistic

effects on adsorption of tetracycline and copper onto a chitosan." *Journal of Colloid and Interface Science*, Vol. 344, No.1, pp.117-125.

Li, W. C., & Wong, M. H. (2015). "A comparative study on tetracycline sorption by Pachydictyon coriaceum and Sargassumhemiphyllum." *International journal of environmental science and technology*, Vol. 12, No. 8, pp. 2731-2740.

Li, Z., Schulz, L., Ackley, C., & Fenske, N. (2010). "Adsorption of tetracycline on kaolinite with pH-dependent surface charges." *Journal of colloid and interface science*, Vol. *351*, No.1, pp. 254-260.

Malik, P. K. (2004). "Dye removal from wastewater using activated carbon developed from sawdust: adsorption equilibrium and kinetics." *Journal of Hazardous Materials*, Vol. 113, No.1-3, pp. 81-88.

Mall, I. D., Srivastava, V. C., & Agarwal, N. K. (2007). "Adsorptive removal of Auramine-O: Kinetic and equilibrium study." *Journal of Hazardous materials*, Vol. 143, No.(1-2), pp. 386-395.

Manigandan, R., Giribabu, K., Suresh, R., Vijayalakshmi, L., Stephen, A., & Narayanan, V. (2013). "Cobalt oxide nanoparticles: characterization and its electrocatalytic activity towards nitrobenzene." *Chemical Science Transactions*, Vol. 2, No.1, pp. 47-S50.

Martins, A. C., Pezoti, O., Cazetta, A. L., Bedin, K. C., Yamazaki, D. A., Bandoch, G. F.,& Almeida, V. C. (2015). "Removal of tetracycline by NaOH-activated carbon produced from macadamia nut shells: kinetic and equilibrium studies." *Chemical Engineering Journal*, Vol. 260, pp. 291-299.

Mote, V. D., Purushotham, Y., & Dole, B. N. (2012). "Williamson-Hall analysis in estimation of lattice strain in nanometer-sized ZnO particles." *Journal of Theoretical and Applied Physics*, Vol.*6*, *No.*1, pp.6.

Parolo, M. E., Savini, M. C., Valles, J. M., Baschini, M. T., & Avena, M. J. (2008). "Tetracycline adsorption on montmorillonite: pH and ionic strength effects." *Applied Clay Science*, Vol. *40*, No. 1-4, pp.179-186.

Roca Jalil, M., Toschi, F., Baschini, M., & Sapag, K. (2018). "Silica Pillared Montmorillonites as Possible Adsorbents of Antibiotics from Water Media." *Applied Sciences*, Vol. 8, No. 8, pp.1403.

Shi, Y., Yang, Z., Wang, B., An, H., Chen, Z., & Cui, H. (2016). "Adsorption and photocatalytic degradation of tetracycline hydrochloride using a palygorskite-supported Cu_2O–TiO_2 composite." *Applied Clay Science*, Vol. 119, pp. 311-320.

Takdastan, A., Mahvi, A. H., Lima, E. C., Shirmardi, M., Babaei, A. A., Goudarzi, G., ... & Vosoughi, M. (2016). "Preparation, characterization, and application of activated carbon from low-cost material for the adsorption of tetracycline antibiotic from aqueous solutions." *Water Science and Technology*, Vol. *74*, No.10, pp. 2349-2363.

Tian, N., Jia, Q., Su, H., Zhi, Y., Ma, A., Wu, J., & Shan, S. (2016). "The synthesis of mesostructured NH 2-MIL-101 (Cr) and kinetic and thermodynamic study in tetracycline aqueous solutions." *Journal of Porous Materials*, Vol. *23*, No. 5, pp. 1269-1278.

Turku, I., Sainio, T., & Paatero, E. (2007). "Thermodynamics of tetracycline adsorption on silica." *Environmental Chemistry Letters*, Vol. *5*, No. 4, pp. 225-228.

Uzunoğlu, D., & Özer, A. (2016). "Adsorption of Acid Blue 121 dye on fish (Dicentrarchus labrax) scales, the extracted from fish scales and commercial hydroxyapatite: equilibrium, kinetic, thermodynamic, and characterization studies." *Desalination and Water Treatment*, Vol. 57, No. 30, pp.14109-14131.

Wu, F. C., Tseng, R. L., & Juang, R. S. (2009). "Initial behavior of intraparticle diffusion model used in the description of adsorption kinetics." *Chemical Engineering Journal*, Vol. 153, No. (1-3), pp.1-8.

Yu, X., Lu, Z., Wu, D., Yu, P., He, M., Chen, T., ... & Feng, Y. (2014). "Heteropolyacid–chitosan/TiO_2 composites for the degradation of tetracycline hydrochloride solution." *Reaction Kinetics, Mechanisms and Catalysis*, Vol.111, No. 1, pp. 347-360.

Zhao, X., Wang, W., Zhang, Y., Wu, S., Li, F., & Liu, J. P. (2014). "Synthesis and characterization of gadolinium doped cobalt ferrite nanoparticles with enhanced adsorption capability for Congo Red." *Chemical Engineering Journal*, Vol. 250, pp.164-174.

Zhao, Y., Geng, J., Wang, X., Gu, X., & Gao, S. (2011). "Adsorption of tetracycline onto goethite in the presence of metal cations and humic substances." *Journal of colloid and interface science*, Vol. 361 No. 1, pp. 247-251.